Supporting Information for

Reversible Topochemical Polymerization and Depolymerization of a Crystalline Three-Dimensional Porous Organic Polymer with C–C Bond Linkages

Chenyue Sun, Julius J. Oppenheim, Grigorii Skorupskii, Luming Yang, Mircea Dincă*

Department of Chemistry, Massachusetts Institute of Technology, Cambridge, Massachusetts 02139, United States
Corresponding Author: mdinca@mit.edu

Table of Contents

General Remarks

All chemicals were purchased from commercial sources and used as received. Tetrakis(4-hydroxyphenyl)methane[1] and 9-anthracenecarbonyl chloride[2] were synthesized according to previous reports. Dry, deaerated tetrahydrofuran was obtained by passing the solvent through two silica columns in a Glass Contour Solvent System. Elemental analyses were performed by Robertson Microlit Laboratories, New Jersey.

Structures in the manuscript were plotted using VESTA 3.[3]

Gas adsorption isotherms were measured by a volumetric method using either a Micromeritics ASAP 2020 Plus or a Micromeritics 2020 gas sorption analyzer. Research grade (Airgas) carbon dioxide and methane were used for the analyses. Samples were activated at 40 °C under high dynamic vacuum (< 10^{-4} mbar) for 24 hours before analysis. An acetone-dry ice slurry was used to maintain the temperature for 195 K analysis while a variable-temperature circulator was used for the analysis at or above 273 K. Oil-free vacuum pumps were used to prevent contamination of sample or feed gases.

Diffuse reflectance infrared Fourier transform spectroscopy (DRIFTS) was performed on a Bruker Tensor 37 (MIR source and KBr beam splitter) with a mercury cadmium telluride (MCT, cooled with liquid nitrogen) detector utilizing the DiffusIR™ accessory (Pike Technologies). To ensure air-free measurement a sealable environmental chamber equipped with ZnSe window (Pike Technologies) was used. The data was averaged over 32 scans between 4000 – 600 cm^{-1} (4 cm^{-1} resolution).

Diffuse reflectance Ultraviolet-visible-near IR spectroscopy (DRUVS) was performed on a Bruker Cary 5000 from 200 to 1000 nm at 600 nm per minute scan rate. The source was switched at 350 nm and the detector was switched at 800 nm. Artefacts caused by the switching was corrected by applying a constant offset in the reflectance. An environmental chamber with quartz window (Pike Technology) was used, together with a UV-vis DiffusIR™ accessory. Thin-film samples were measured on the same instrument using a blank quartz slide as reference in dual-beam transmission mode.

For thin film fabrication, the substrate (glass or quartz) was first sonicated in water, acetone and isopropanol, in that order, and dried under a flow of nitrogen. MTBA was dissolved in chlorobenzene at 10 mg/mL concentration and filtered through a PTFE syringe filter. 20 μL of the solution was dropped at the center of the substrate, which was then spun at 1000 rpm for 6 seconds and at 4000 rpm for 30 seconds. The spin-coating process was repeated 5 times to increase the thickness of the film. The as-deposited thin film is amorphous by GIXRD. To increase the crystallinity, a glass Petri dish was covered with chlorobenzene. The spin-coated substrate was attached to a larger Petri dish, which was then placed above the first dish so that the substrate is in contact with solvent vapor. The annealing was set undisturbed for 24 – 72 hours until crystals can be observed under optical microscope.

Atomic force microscopy was performed at the Institute for Soldier Nanotechnologies (ISN) on a Veeco Dimension 3100 AFM in tapping mode. An Sb-doped Si tip (RTESPA-150, Bruker) was used.

Photoluminescence was measured with a 365 nm LED (Thorlabs) as excitation source. The luminescence was filtered with a 400 nm long-pass filter (Thorlabs) and focused on a fiber connected to spectrometer (Princeton Instruments SP2300 and PIXIS-100). For powder samples, the sample was sandwiched between two quartz slides. For thin film samples, the sample was deposited onto a quartz slide by spin-coating.

Solution ^{1}H and ^{13}C **nuclear magnetic resonance spectroscopy (NMR)** was measured on a 500 MHz JEOL JNM-ECZ500R/S1 or a 400 MHz Bruker Avance-III HD Nanobay or a 400 MHz Bruker Avance Neo spectrometer. Solid-state NMR was measured on a Bruker Avance Neo spectrometer (500 MHz) with a 3.2mm HX solids probe. For ^{13}C experiments, the multiCP[4] pulse sequence was used for supplementary fig. 6 while regular CP pulse was used for supplementary fig 16. For the stability test, the sample was stored in the fridge (4 °C) prior to the first measurement, and under ambient condition inside the rotor in between each successive measurement. For quantitative ^{1}H experiments, the windowed phase-modulated Lee–Goldburg (wpmlgd2)[5] pulse sequence was used. Chemical shift of ^{1}H NMR spectra was calibrated using an internal standard of malonic acid, which was mixed in after the sample spectra were taken. The peaks corresponding to malonic acid are calibrated to 13.0 and 2.8 ppm.[6]

X-ray crystallography

Powder X-ray diffraction (PXRD) patterns were recorded with a Bruker Advance II diffractometer equipped with a θ/2θ reflection geometry and Ni-filtered CuKα radiation ($K\alpha_1$ = 1.5406 Å, $K\alpha_2$ = 1.5444 Å, $K\alpha_2$/ $K\alpha_1$ = 0.5). The tube voltage and current were 40 kV and 40 mA, respectively. Samples for PXRD were prepared by placing a thin layer of the appropriate material on a zero-background silicon crystal plate. Variable-temperature PXRD patterns were measured on a Rigaku Smartlab diffractometer in the X-ray diffraction shared experimental facility of the MIT Materials Research Science and Engineering Center. The powder sample was placed on an Al_2O_3 sample holder (Anton Paar). The diffractometer was configured in variable-slit Bragg-Brentano mode with an irradiated length of 6 mm, with a Cu anode X-ray source, and a D/teX 1D detector. The heating chamber was constantly purged with helium and the temperature was

ramped at a rate of 5 °C/min. The diffractograms were converted into constant-slit-width intensities using HighScore Plus. For grazing-incidence XRD, the same Rigaku Smartlab instrument was used with a parallel-beam setup.

High resolution synchrotron powder diffraction data were collected using the mail-in service of the beamline 11-BM[7] at the Advanced Photon Source, Argonne National Laboratory, using an average wavelength of 0.458107 Å. Powder of polyMTBA was dried under dynamic vacuum at room temperature, and packed in air into a Kapton capillary provided by 11-BM. The PXRD pattern was then collected at 100 K. The pattern was indexed in TOPAS-Academic,[8] giving the best fits to the space group $I4_1/a$ (88) and its extinction equivalents. The PXRD pattern was then fitted with the unit cell parameters of the produced model, using Pawley refinement as implemented in TOPAS-Academic. Minor anisotropy in peak widths was corrected for as anisotropic strain broadening according to the model by Stephens et al for a tetragonal unit cell.[9] The results of the refinement are presented in Supplementary table 1.

Low-temperature single-crystal diffraction data were collected on a Bruker-AXS D8 Venture Kappa Duo diffractometer coupled to a Photon III CPAD detector, using Cu Kα radiation (λ = 1.54178 Å) from an IμS 3.0 microfocus source, performing φ-and ω-scans. A crystal of the polymer was submerged in Paratone oil, and mounted on a MiTeGen crystal loop. Diffraction data were integrated using SAINT (Bruker-AXS), and absorption correction and scaling were performed using SADABS (Bruker-AXS). The SHELX suite[10] was used for structure solution and refinement. The structure was solved using SHELXT[11] and refined against F^2 on all data by full-matrix least squares with SHELXL following established refinement strategies. All non-hydrogen atoms were refined anisotropically. Hydrogen atoms were refined using the riding model. Selected information regarding the refinement is presented in Supplementary table 2.

Level A and B alerts in checkCIF:

PLAT094_ALERT_2_B Ratio of Maximum / Minimum Residual Density .... 4.95 Report

Response: Strong residual maximum (1.15 eA-3) was located too close to the molecule to be part of disordered solvent, and no clear twinning was observed. The issue is likely due to poor crystal quality and small size.

PLAT097_ALERT_2_B Large Reported Max. (Positive) Residual Density 1.15 eA-3

Response: Strong residual maximum (1.15 eA-3) was located too close to the molecule to be part of disordered solvent, and no clear twinning was observed. The issue is likely due to poor crystal quality and small size.

Computation Details

All calculations were performed using the Biovia Materials Studio 2020 software, with the Forcite module for molecular mechanics geometry optimizations. Molecular mechanics geometry optimizations were performed using the COMPASS III force field[12] using QEq charges[13], using cell parameters as determined by Pawley refinement of the experimental PXRD pattern. The COMPASS III force field was chosen as relaxed structures yielded more physically accurate bond lengths (when compared to structures in the Cambridge Structural Database) than the structures relaxed with other force fields. Isomers for polyMTBA whereby the orientation of the ester functional groups rotate by 180° were considered, however resulted in higher energy configurations.

Simulations of sorption properties were performed using RASPA v2.0 using the GenericMOFs force field to describe the interaction between CO_2 and the framework.[14] Partial charges on the atoms were calculated using the charge equilibration scheme developed by Wilmer and Snurr.[15] Uptake capacity at 273 K and 1 bar was determined using a Monte Carlo simulation with 10000 cycles, and the CO_2 surface area was determined using 1000 cycles.

A virial analysis[16] was used to determine the isosteric enthalpy of adsorption. The adsorption data at all three temperatures were fit simultaneously using the virial model, $\log P = \frac{1}{T}\sum_{i=0}^{6} a_i n^i + \sum_{j=0}^{1} b_i n^i + \log n$ and the isosteric enthalpy of adsorption where calculated from the temperature dependent parameters, $\Delta H = R\sum_{i=0}^{6} a_i n^i$. Where P is pressure, T is temperature, n is quantity adsorbed, R is the ideal gas constant, ΔH is the isosteric enthalpy of adsorption, and a_i and b_i are temperature dependent and independent parameters. Error bars were calculated by error propagating from uncertainty in each parameter.

Experimental Details

Synthesis of methanetetrayltetrakis(benzene-4,1-diyl) tetrakis(anthracene-9-carboxylate) (MTBA)

In order to avoid unintended photodimerization, the synthesis was carried out with minimal light exposure. In a nitrogen-filled glove box, 125 mg NaH (5.2 mmol, 20 equiv.) and 100 mg tetrakis(4-hydroxyphenyl)methane (0.26 mmol, 1 equiv.) were charged into a 250 mL Schlenk flask. The flask was then sealed and removed from the box. Under nitrogen, dry THF (10 mL) was added and the flask was chilled to 0 °C with an ice-water bath. In a separate flask, 376 mg 9-anthracenecarbonyl chloride (1.56 mmol, 6 equiv.) was dissolved in 10 mL THF under nitrogen. The acid chloride solution was added dropwise into the other flask, over the course of 30 minutes. The mixture was slowly warmed to room

temperature and stirred under nitrogen for 2 days, during which the mixture turned orange. THF was then removed under reduced pressure at 30 °C and 20 mL saturated $NaHCO_3$ aqueous solution was added into the flask. The suspension was extracted with dichloromethane three times and the organic phase was separated and dried over $MgSO_4$. After the solution was concentrated in vacuo, recrystallization from DCM/Methanol afforded MTBA as a polycrystalline yellow powder. Yield: 220 mg (70.4%) ^{1}H NMR (400 MHz, CD_2Cl_2): δ 8.66 (s, 4H), 8.29 (d, J = 8.7 Hz, 8H), 8.12 (d, J = 8.7 Hz, 8H), 7.70 – 7.60 (m, 16H), 7.60 – 7.50 (m, 16H). ^{13}C NMR (101 MHz, CD_2Cl_2) δ 168.13, 149.72, 144.83, 132.61, 131.40, 130.60, 129.18, 129.03, 127.90, 126.92, 126.09, 125.11, 121.59, 64.36. HRMS (ESI+): calculated m/z for $C_{85}H_{52}O_8Na^+$: 1223.3560, found 1223.3537; EA: found C 82.05% H 4.24% calculated for $C_{85}H_{52}O_8 \cdot 0.61\ CH_2Cl_2$: C 82.05% H 4.28%. Single crystals were grown by layering over a 0.5 mg/mL DCM solution with pentane. We have found the purity of the recrystallized product to be satisfactory for most purposes, and we note higher purity can be achieved by column chromatography (basic alumina, DCM:hexane 2:1, Rf = 0.78) at cost of yield.

Photopolymerization of MTBA

45 mg MTBA was suspended in 20 mL diethyl ether in a cylindrical Schlenk tube. The mixture was degassed with three freeze-pump-thaw cycles, after which it was refilled with 1 bar CO_2 through a Schlenk line. A 427 nm LED (PR-160L, Kessil) was placed 1 cm away from the Schlenk tube and an electrical fan was used to cool the LED. The mixture was stirred at room temperature for 3 days, during which the green emission turned into faint sky blue and solids turned from bright yellow to beige. Afterwards, the solids were separated by centrifugation and evacuated under vacuum. Yield: 44.5 mg (99%) EA: found C 82.49% H 4.05% calculated for $C_{85}H_{52}O_8 \cdot 1.24\ CO_2$: C82.48% H 4.17%. The CO_2 in the formula could be a result of kinetically trapped carbon dioxide or photochemical carboxylation.

Thermolysis of polyMTBA

10.5 mg of polyMTBA was sealed in a ¼ inch glass tube under vacuum. The tube was then placed in an oven and heated at 180 °C for 12 hours. After cooling to room temperature, the tube was opened under air and the residue was dissolved in ca 2 mL of dichloromethane and passed through a short plug of alumina. Pentane was then layered on top to induce crystallization. Bright yellow needles were collected by decanting and dried under vacuum. Yield 3.0 mg (29%)

Supplementary figure 1. Close-up view of the anthracene pairs in MTBA

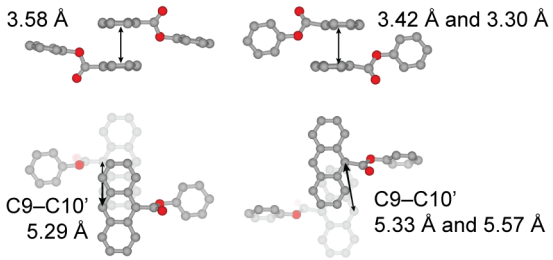

There are two distinct anthracene pairs in the asymmetric unit (shown above). The pair on the right is also disordered over two positions (45:55) and therefore two sets of distances are given.

Supplementary figure 2. Photoluminescence spectra of MTBA powder

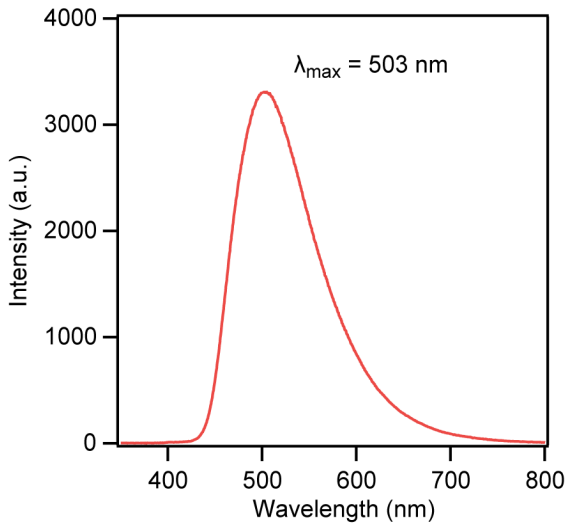

Supplementary figure 3. CO_2 adsorption isotherm of MTBA at 273 K

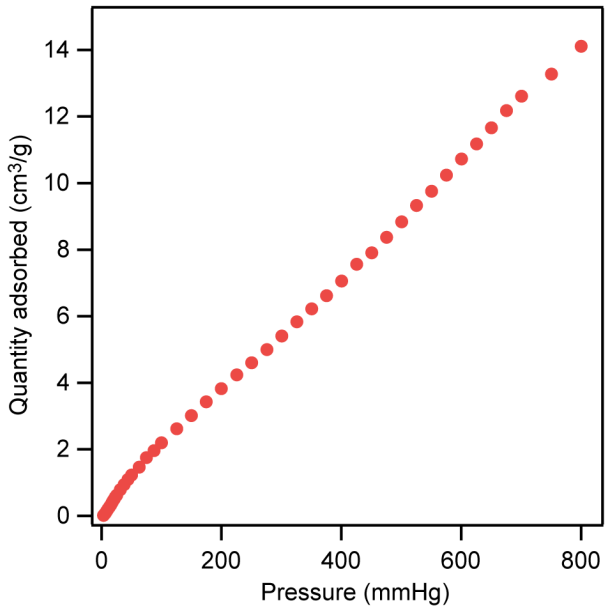

Supplementary figure 4. Diffuse reflectance UV-Visible spectra (DRUV) of powder MTBA and polyMTBA

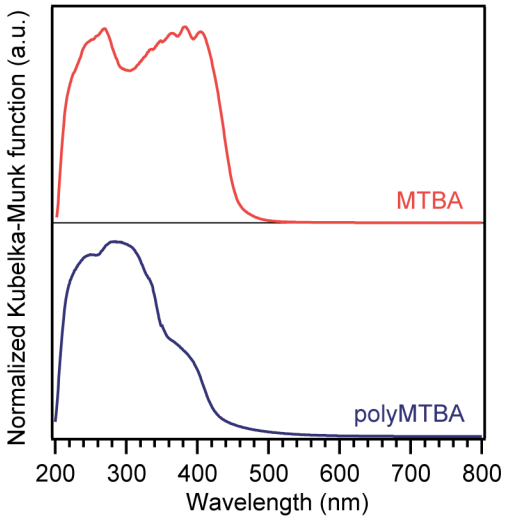

It should be noted that diffuse-reflectance method is usually not quantitative, and the data should only be assessed qualitatively.

Supplementary figure 5. Diffuse reflectance infrared spectra (DRIFTS) of MTBA and polyMTBA

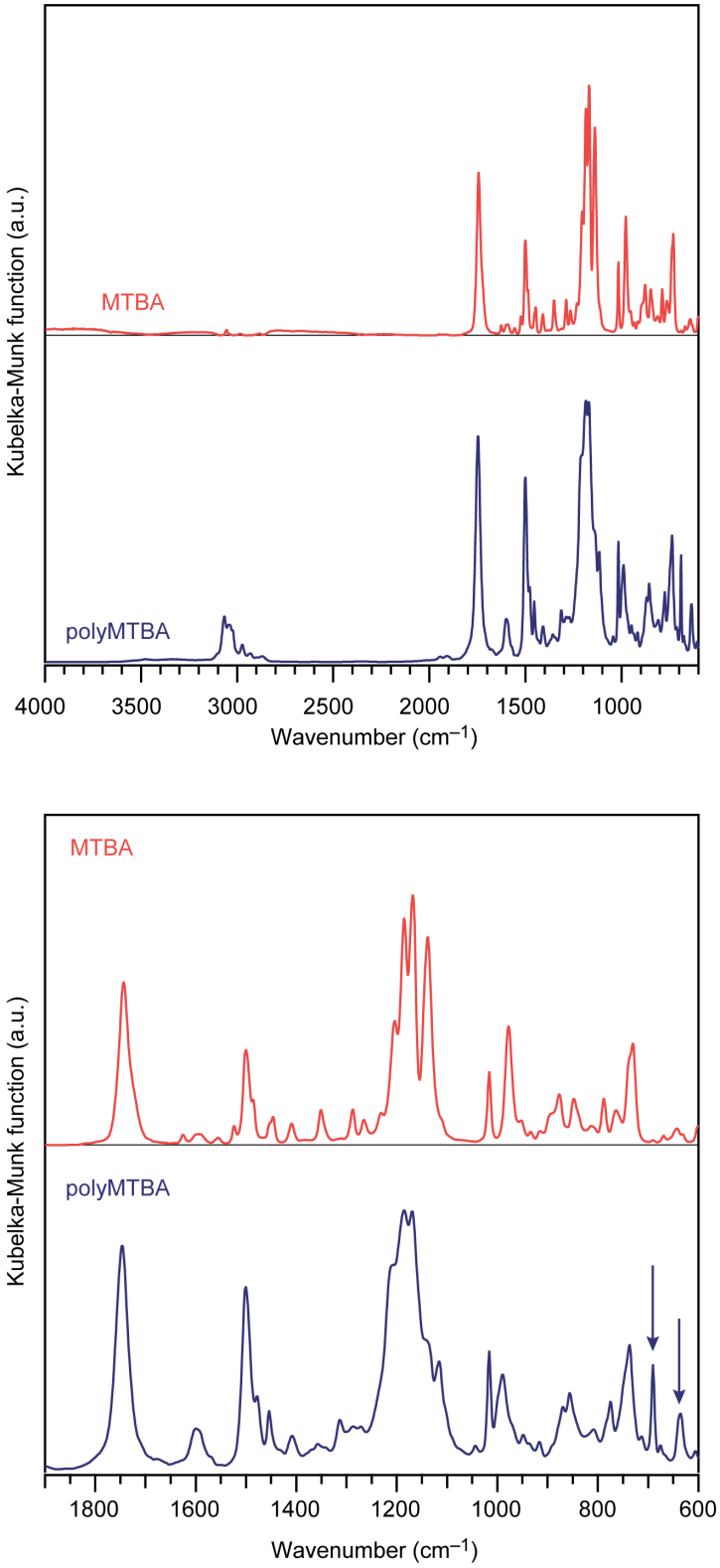

The lower wavenumber region is magnified in the bottom figure to highlight the peaks characteristic of dianthracenes (denoted with arrow).

Supplementary figure 6. ^{13}C solid-state CP-MAS NMR of MTBA and polyMTBA

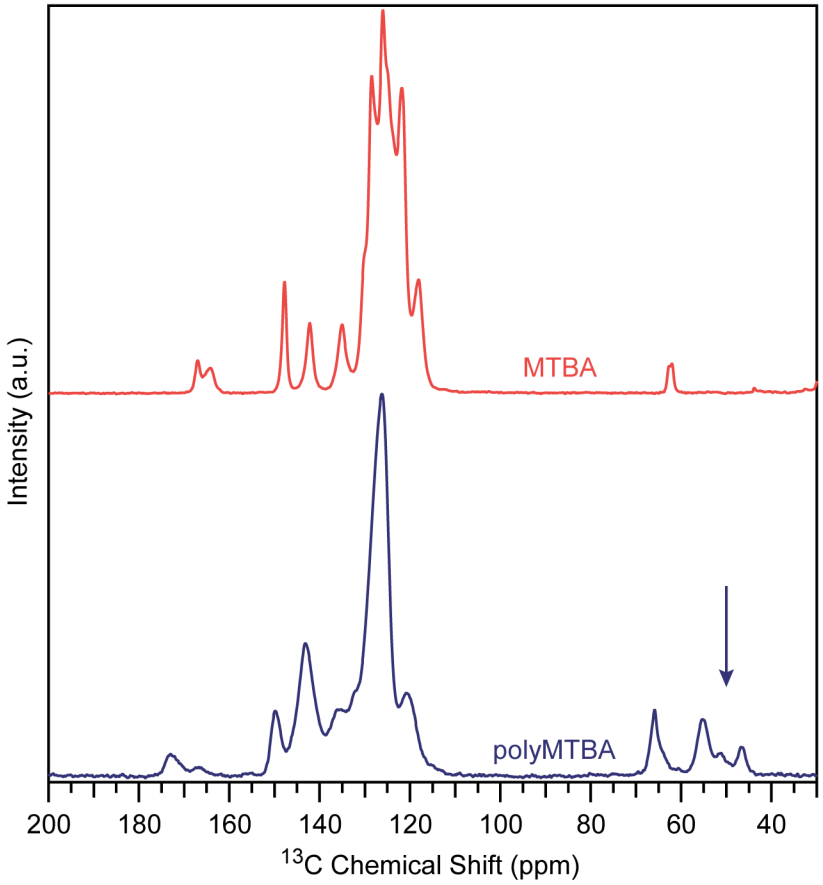

The spinning side bands are outside the spectral window presented. The peaks from bridgehead carbon (~ 50 ppm) in the polymer are marked with an arrow.

Supplementary figure 7. Scanning electron microscope (SEM) images of MTBA and polyMTBA.

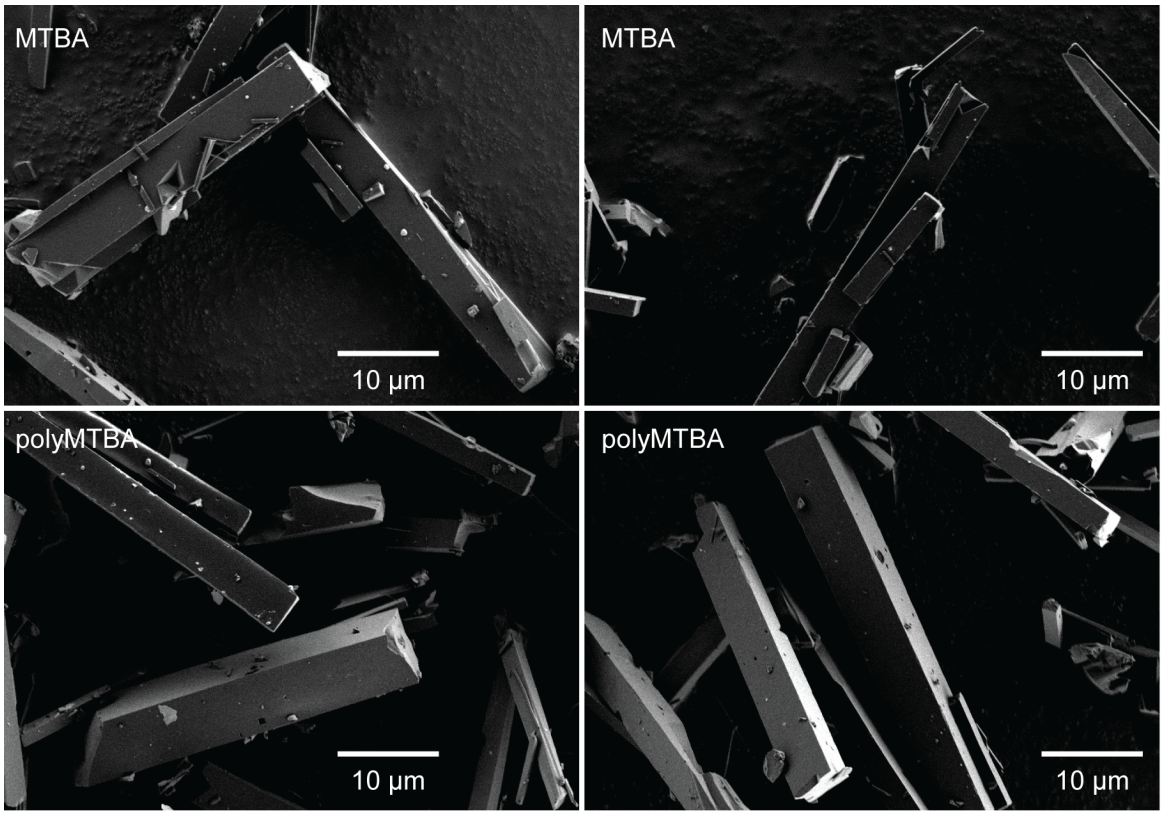

Supplementary figure 8. Pawley refinement of polyMTBA synchrotron powder X-ray diffraction pattern

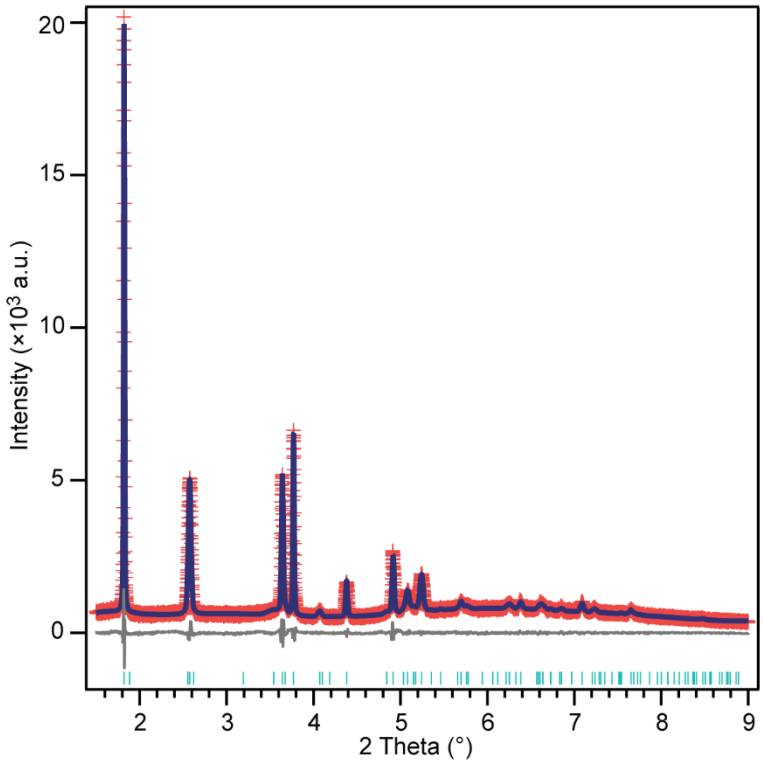

Experimental intensity (Red markers), refined intensity (blue trace), difference intensity (gray trace), and expected Bragg diffraction positions (turquoise marker)

Supplementary table 1. Details of the Pawley refinement of synchrotron PXRD data for polyMTBA

	polyMTBA
Space group	$I4_1/a$ (88)
a/Å	28.8432(3)
c/Å	15.9068(2)
V/Å^3	13233.3(2)
R_{wp}	0.0468
R_{exp}	0.0417
GoF	1.12
2θ range	1.5 – 9°
Wavelength/ Å	0.458107
Temperature/ K	100

Supplementary table 2. Details of the crystal structure refinement for MTBA

Identification code	**2084357**
Empirical formula	$C_{85}H_{52}O_8$
Formula weight	1201.26
Temperature/K	100(2)
Crystal system	tetragonal
Space group	$I4_1/a$
a/Å	28.2999(3)
b/Å	28.2999(3)
c/Å	15.0898(2)
α/°	90
β/°	90
γ/°	90
Volume/Å³	12085.2(3)
Z	8
ϱ_{calc}g/cm³	1.320
μ/mm⁻¹	0.669
F(000)	5008.0
Crystal size/mm³	0.22 × 0.08 × 0.06
Radiation	CuKα (λ = 1.54178)
2Θ range for data collection/°	6.246 to 141.488
Index ranges	-34 ≤ h ≤ 34, -34 ≤ k ≤ 34, -18 ≤ l ≤ 18
Reflections collected	100149
Independent reflections	5784 [R_{int} = 0.0402, R_{sigma} = 0.0138]
Data/restraints/parameters	5784/1683/627
Goodness-of-fit on F²	1.479
Final R indexes [I>=2σ (I)]	R_1 = 0.0943, wR_2 = 0.3059
Final R indexes [all data]	R_1 = 0.1058, wR_2 = 0.3308
Largest diff. peak/hole / e Å⁻³	1.15/-0.23

Supplementary figure 9. Computed structure of polyMTBA.

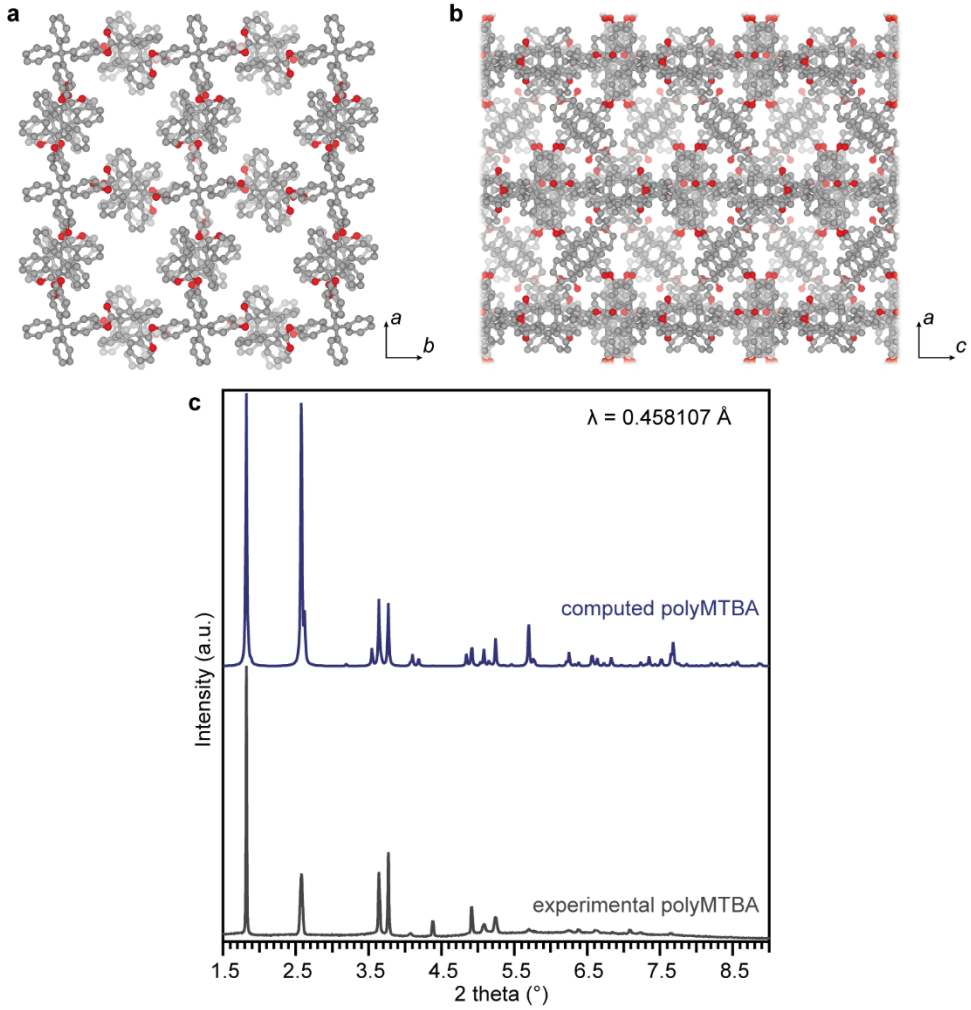

Lattice parameters from Pawley refinement were used to construct the initial guess for polyMTBA structure, which was then optimized using COMPASS III forcefield[12] with Qeq charges. The polymer framework is (a) microporous along the *c*-direction and (b) nonporous along a- or *b*-direction. A comparison of the powder X-ray diffraction patterns from the computed polymer structure and experimental data is provided in (c).

Supplementary figure 10. Atomic Force Microscope image of polyMTBA on glass

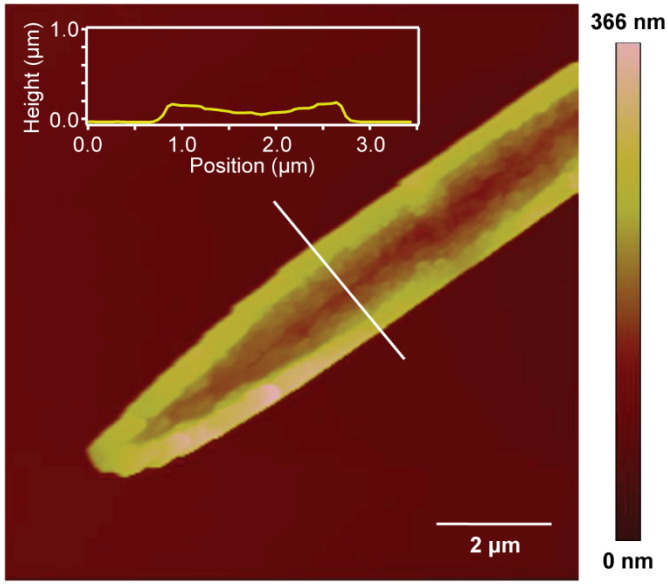

polyMTBA was deposited onto glass substrate via spin-coating followed by solvent vapor annealing. The inset shows the height profile at the cross section denoted by the white line. The low height of the spindle suggests that it is embedded in a matrix of polyMTBA rather than free standing. Color code for the AFM-determined height is shown on the right.

Supplementary figure 11. CO_2 adsorption isotherm of polyMTBA at 195 K and 273 K

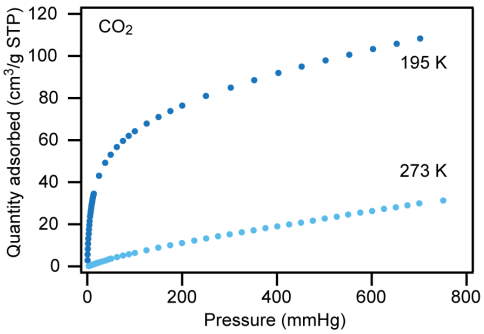

Supplementary figure 12. Isosteric heat of adsorption (CO_2)

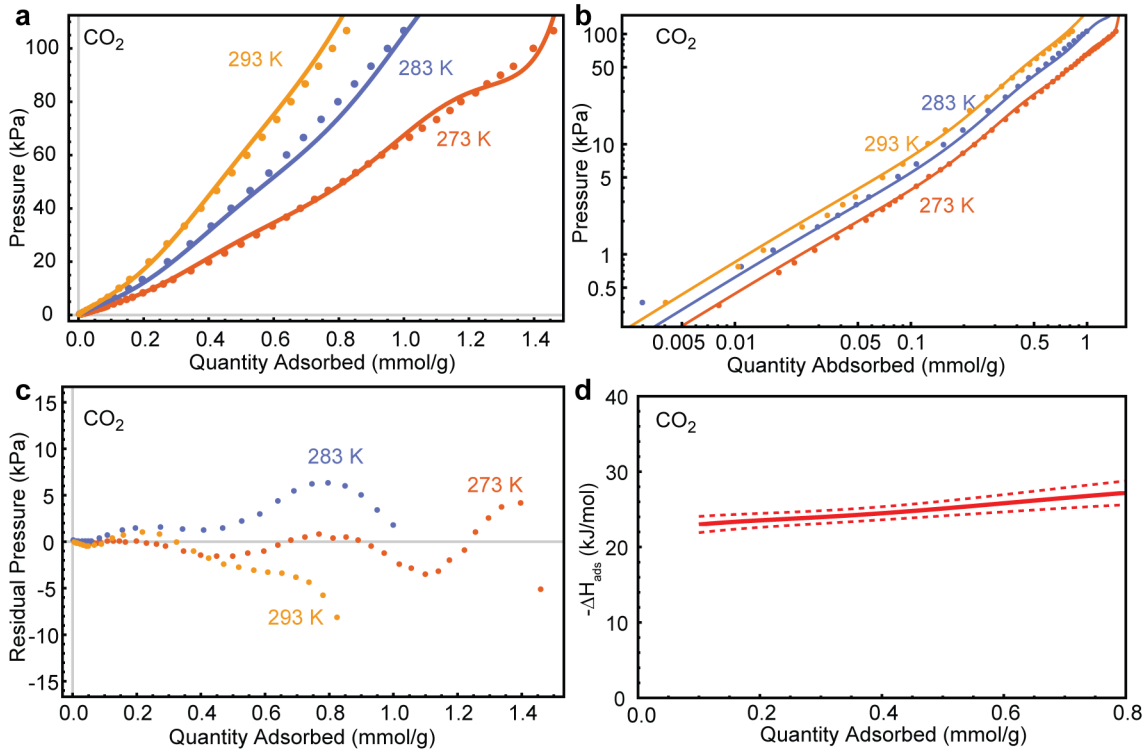

Virial fitting (solid line, $R^2 = 0.999173$) of experimental isotherms (dot) of CO_2 on polyMTBA at three temperatures on linear scale (a) and logarithmic scale (b). The difference between experimental and modeled data is also plotted (c). The isosteric heat of adsorption is calculated based on Clausius-Clapeyron equation (solid line, d) and shown with the confidence interval (dotted lines). |ΔH| at 0.1 mmol/g is 22.99 ± 1.07 kJ/mol (bottom right).

Supplementary figure 13. Thermogravimetric analyses of MTBA and polyMTBA

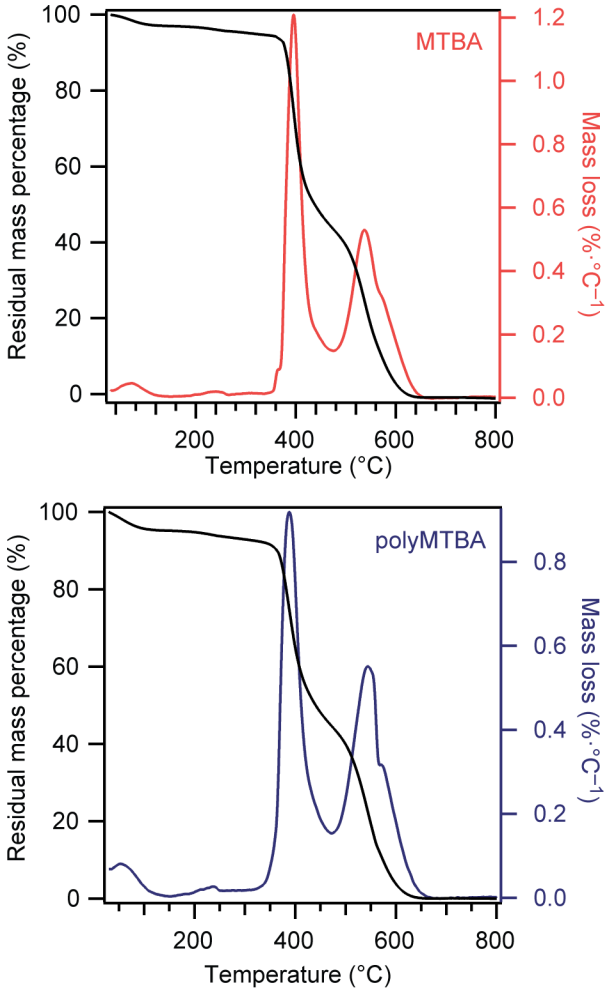

Supplementary figure 14. Variable-temperature PXRD of polyMTBA

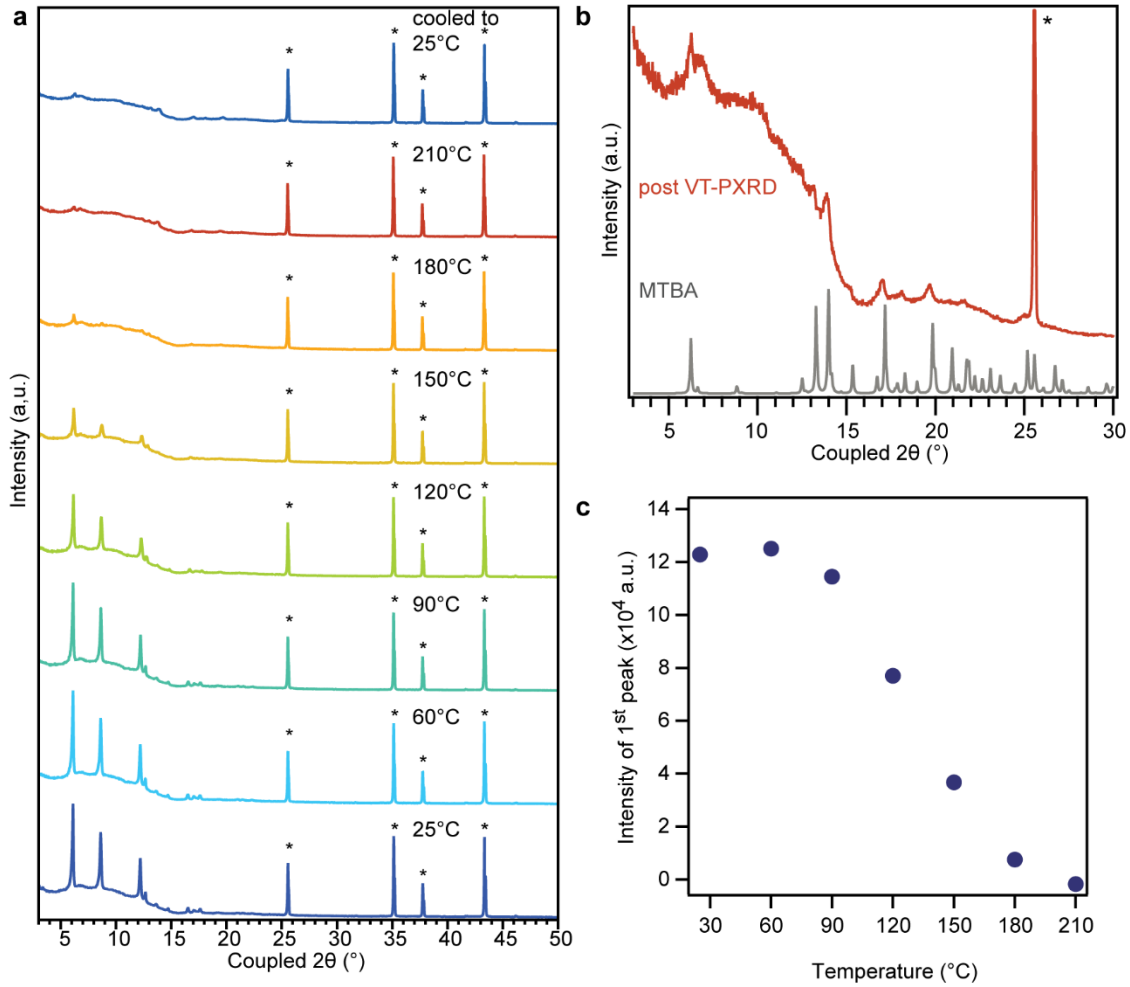

(a) The sample was heated in a flow of helium at 5 °C/min. Temperature was held constant during each scan. Peaks from the alumina holder are labeled with asterisks. (b) Comparison of the pattern of thermolysis and the pattern of MTBA (simulated). (c) The intensity of the first peak versus temperature. The intensity at 210 °C was taken as the background intensity and subtracted from rest of the data points. The change in intensity is a result of both depolymerization and thermal broadening.

Supplementary figure 15. NMR of VTPXRD sample

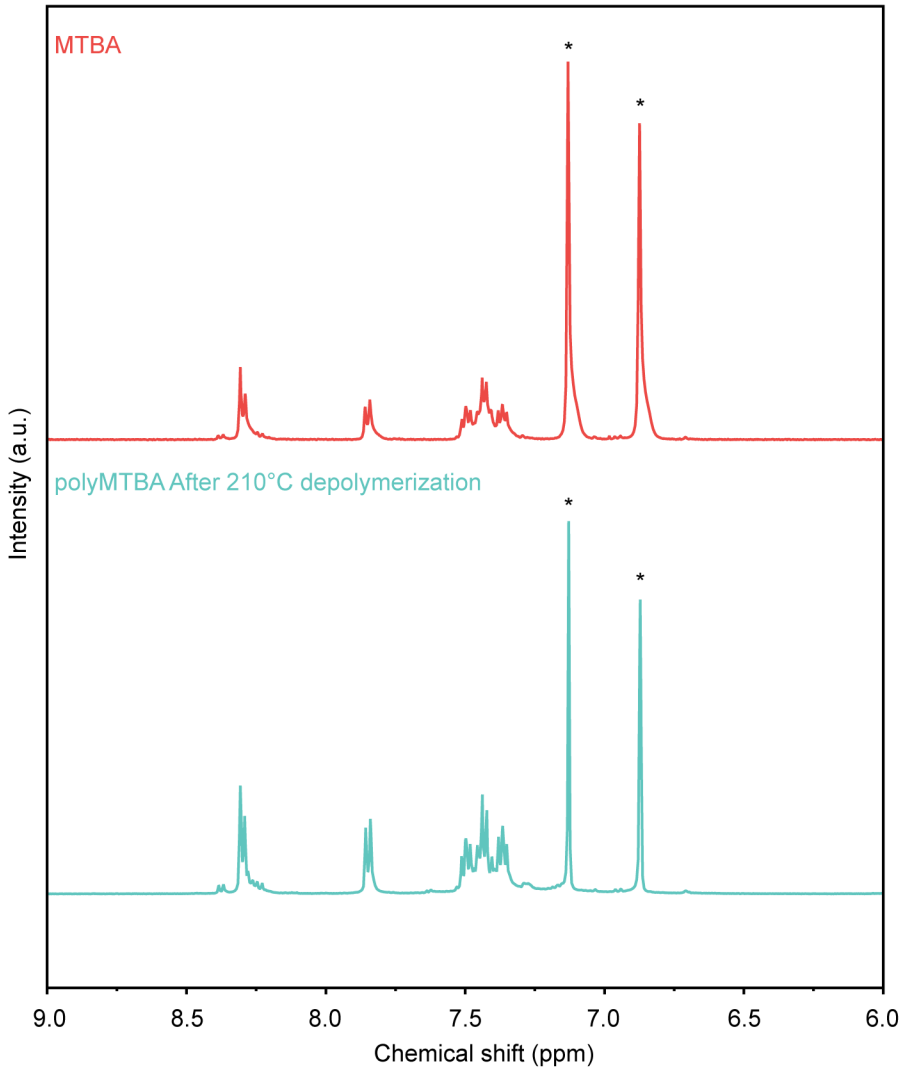

Residual solvent signals (dichlorobenzene) are marked with asterisks.

Supplementary figure 16. PXRD and optical microscope image of recycled MTBA

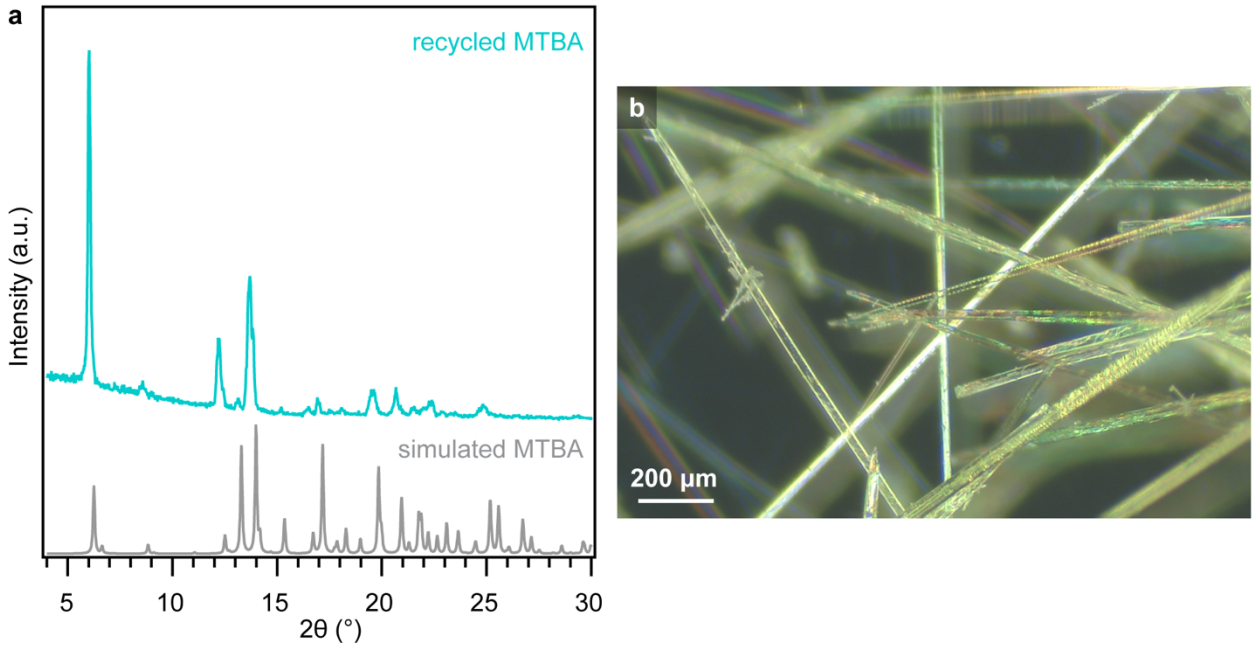

The thermolysis product of polyMTBA was dissolved in CH_2Cl_2, passed through a plug of basic alumina and recrystallized from CH_2Cl_2/pentane. (a) PXRD of the recycled MTBA. The difference in intensity is likely caused by preferred orientation as the recrystallized monomers are long, fine needles, as shown in (b) the optical microscope image.

Supplementary figure 17. DSC of polyMTBA

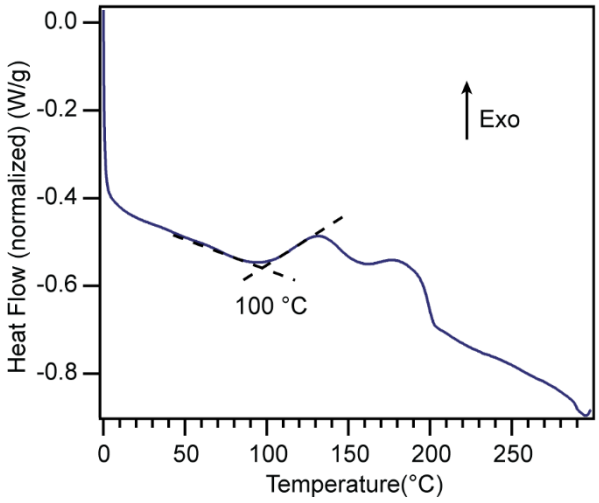

Supplementary figure 18. Solid-state ^{13}C-NMR spectrum of polyMTBA stored under ambient condition

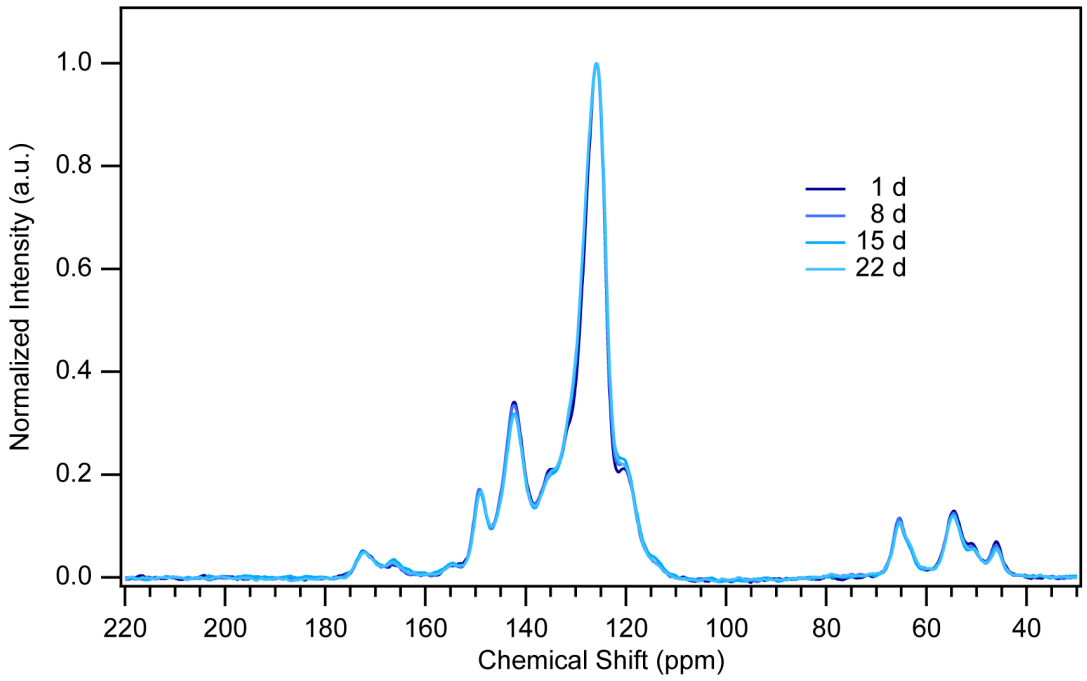

Reference

1. Meng, M. *et al.* Two Base Pair Duplexes Suffice to Build a Novel Material. *ChemBioChem* **10**, 1335–1339 (2009).
2. Connal, L. A., Vestberg, R., Hawker, C. J. & Qiao, G. G. Fabrication of Reversibly Crosslinkable, 3-Dimensionally Conformal Polymeric Microstructures. *Adv. Funct. Mater.* **18**, 3315–3322 (2008).
3. Momma, K. & Izumi, F. VESTA 3 for three-dimensional visualization of crystal, volumetric and morphology data. *J. Appl. Crystallogr.* **44**, 1272–1276 (2011).
4. Johnson, R. L. & Schmidt-Rohr, K. Quantitative solid-state 13C NMR with signal enhancement by multiple cross polarization. *J. Magn. Reson.* **239**, 44–49 (2014).
5. Leskes, M., Madhu, P. K. & Vega, S. A broad-banded z-rotation windowed phase-modulated Lee-Goldburg pulse sequence for 1H spectroscopy in solid-state NMR. *Chem. Phys. Lett.* **447**, 370–374 (2007).
6. Schnell, I. & Spiess, W. H. High-resolution 1H NMR spectroscopy in the solid state: Very fast sample rotation and multiple-quantum coherences. *J. Magn. Reson.* **151**, 153–227 (2001).
7. Lee, P. L. *et al.* A twelve-analyzer detector system for high-resolution powder diffraction. *J. Synchrotron Radiat.* **15**, 427–432 (2008).
8. Coelho, A. Topas Academic v6. *Coelho Softw.* (2017).
9. Stephens, P. W. Phenomenological model of anisotropic peak broadening in powder diffraction. *J. Appl. Crystallogr.* **32**, 281–289 (1999).
10. Sheldrick, G. M. A short history of SHELX. *Acta Crystallographica Section A: Foundations of Crystallography* **64**, 112–122 (2008).
11. Sheldrick, G. M. SHELXT - Integrated space-group and crystal-structure determination. *Acta Crystallogr. Sect. A Found. Crystallogr.* **71**, 3–8 (2015).
12. Akkermans, R. L. C., Spenley, N. A. & Robertson, S. H. COMPASS III: automated fitting workflows and extension to ionic liquids. *Mol. Simul.* 1–12 (2020). doi:10.1080/08927022.2020.1808215
13. Rappe, A. K. & Goddard, W. A. Charge equilibration for molecular dynamics simulations. *J. Phys. Chem.* **95**, 3358–3363 (1991).
14. Dubbeldam, D., Calero, S., Ellis, D. E. & Snurr, R. Q. RASPA: molecular simulation software for adsorption and diffusion in flexible nanoporous materials. *Mol. Simul.* **42**, 81–101 (2016).
15. Wilmer, C. E., Kim, K. C. & Snurr, R. Q. An Extended Charge Equilibration Method. *J. Phys. Chem. Lett.* **3**, 2506–2511 (2012).
16. Nuhnen, A. & Janiak, C. A practical guide to calculate the isosteric heat/enthalpy of adsorption via adsorption isotherms in metal–organic frameworks, MOFs. *Dalton Trans.* **49**, 10295–10307 (2020).